Multiple-ionization channels in proton-atom collisions

R. D. DuBois
Pacific Northwest Laboratory, Richland, Washington 99352

Steven T. Manson
Department of Physics and Astronomy, Georgia State University, Atlanta, Georgia 30303
(Received 30 October 1986)

A detailed investigation of multiple ionization of He (ionization charge states $q=1,2$), Ne ($q=1-3$), and Ar and Kr ($q=1-4$) is presented for proton impact energies ranging from 10 keV to a few MeV. Absolute cross sections for various ionization pathways have been obtained by combining some new measurements with previously published experimental results and, in certain cases, with existing theoretical information. It is shown how each of these pathways contribute to the various stages of target ionization that are observed after the collision and how these experimentally measured quantities are related to the cross sections for initial inner- and outer-shell vacancy production. Areas where additional data are required or where the existing data are not internally consistent are pointed out. In general, it is shown that the existing data are sufficient to describe the ionization of helium as well as the lower levels of ionization of neon, argon, and krypton. However, for the higher degrees of ionization, particularly for Kr, our understanding is hampered by substantial gaps in the available inner-shell ionization data—both in cross-section and branching-ratio information. Nevertheless, the data are sufficient to indicate the relative importance of the various pathways. For all targets, direct multiple outer-shell cross sections were extracted. Analyzing the energy dependences of these cross sections provided some hints as to how to calculate multiple-ionization cross sections, e.g., information as to where the multiple ionization is dominated by the first-order or by a higher-order term in the perturbation expansion of the proton-target interaction is obtained.

I. INTRODUCTION

Multiple ionization has long been recognized as an important process in ion-atom collisions. While our understanding of single ionization induced by bare charged particles is reasonably good, the situation is otherwise for multiple ionization. Part of the problem is that there are, in general, many ionization pathways leading to a particular stage of ionization of an atom. For example, measured total multiple-ionization cross sections can result from (a) direct multiple outer-shell ionization, (b) single or double charge transfer with possible simultaneous additional ionization, and (c) inner-shell ionization followed by Auger (or x-ray) relaxation; this relaxation can produce additional ionization via Auger cascades. In addition, initial inner-shell ionization can be accompanied by simultaneous outer-shell ionization or can decay via multiple Auger processes. In the latter case, one electron drops down to fill a hole and two (or more) electrons are ejected. Untangling these ionization pathways is a necessary first step in rendering multiple-ionization cross sections amenable to theoretical interpretation and, ultimately, lead to reliable theoretical predictions.

In this paper, we report on our attempts to unravel the complex multiple-ionization process for proton-impact ionization of the noble gases: helium, neon, argon, and krypton. Proton impact was chosen since the situation is not made more complicated by the presence of projectile electrons. In addition, there is a fair amount of experimental data available on multiple ionization by proton impact; some new data are being reported in this paper. Since the majority of the past and present data involves noble gases, these are the targets considered in this work.

Basically, the aims of this paper are fourfold. First, we indicate how various initial target vacancies, created via direct ionization or charge transfer, lead to different degrees of target ionization. Also, to show how these initial vacancies are related to (a) experimentally obtained cross sections where the final charge states of the target and/or projectile are measured and (b) how they relate to experimentally measured inner-shell vacancy production cross sections. The second aim is to obtain cross sections for the various individual processes (ionization pathways) that contribute to the total multiple ionization cross section. These cross sections for the various pathways were taken directly from the literature or were indirectly obtained by combining various types of information (e.g., relative charge-state measurements, total cross sections, Auger branching ratios, etc.). Third, we make some attempt at a theoretical interpretation of the individual cross sections leading to direct multiple outer-shell ionization in order to evaluate how to calculate these cross sections theoretically. Fourth, we point out gaps or inconsistencies in the experimental data in an effort to stimulate specific measurements which will significantly enhance our understanding of multiple ionization in ion-atom collisions.

In this paper, a number of different types of cross sections are referred to in analyzing the various pathways

leading to multiple ionization. Hence, an exposition of the notation used in this paper is necessary. Unfortunately, no universally accepted notation has been established in the literature, so we have adopted a notation that is as general and easy to use as possible but yet is specific enough to clearly designate the various cross sections used in this paper. These cross sections are denoted as follows. σ_+ is the total target positive-charge-production cross section; σ_- is the total target electron-production cross section; σ_q^T is the total cross section for producing target ions of charge $+q$; σ_q^{ij} is the cross section for producing target charge $+q$ with the initial and final projectile charge states i and j, respectively; σ^{ij} is the total charge-transfer cross section where the initial and final projectile charge states are i and j, respectively, and the target charge state is unknown; σ_A^T is the total vacancy-production cross section for shell A; σ_A^{ij} is the vacancy-production cross section for shell A where the initial and final charge states of the projectile are i and j; and $\sigma_{AB^n}^T$, $\sigma_{AB^n}^{ij}$ are the cross sections for producing a vacancy in shell A along with n vacancies in shell B. The superscripts are defined as above.

These cross sections are interrelated in the following manner:

$$\sigma_q^T = \sum_j \sigma_q^{ij} , \tag{1}$$

$$\sigma^{ij} = \sum_q \sigma_q^{ij} , \tag{2}$$

$$\sigma_+ = \sum_q q\sigma_q^T = \sum_{q,j} q\sigma_q^{ij} , \tag{3}$$

$$\sigma_- = \sum_{q,j} (q + j - i)\sigma_q^{ij} . \tag{4}$$

The difference between σ_+ and σ_- is, of course, the charge-transfer processes (σ^{10} and σ^{1-1}) which create more target ions than electrons. It is thus clear that for proton impact $\sigma_+ > \sigma_-$.

At a more fundamental level the cross section for a particular vacancy state, e.g., KL, is written as σ_{KL}^{ij} or σ_{KL}^T, as defined above. These vacancy states account for the initial process only; they are followed by Auger or x-ray relaxation. Thus to relate these fundamental cross sections to the measurable quantities defined above requires knowledge of fluorescence yields and Auger branching ratios. In general, past measurements of inner-shell vacancy states have not discriminated between single-vacancy production and an inner-shell vacancy created along with outer-shell vacancies. Such cross sections are denoted by $\sigma_{\bar{K}}^{ij}$ or $\sigma_{\bar{K}}^T$ for K vacancies. For example,

$$\sigma_{\bar{K}}^{ij} = \sum_{n=0}^{8} \sigma_{KL^n}^{ij} . \tag{5}$$

It is important to distinguish this $\sigma_{\bar{K}}^{ij}$ from σ_K^{ij} which is identically the same as $\sigma_{KL^0}^{ij}$ if we explicitly denote that no outer-shell vacancies accompany the inner-shell ionization.

Of particular interest in this paper are the cross sections for direct (as opposed to charge transfer) multiple outer-shell ionization of the target. These cross sections differ from the measured σ_q^{11} cross sections which contain contributions from direct multiple outer-shell *and* from direct inner-shell ionization followed by Auger relaxation. The inner-shell component must be subtracted to obtain the outer-shell contribution. In order to determine the direct multiple outer-shell cross sections then, accurate values for σ_q^{11} are required. These were obtained from the literature and supplemented with some additional measurements that we have performed for argon targets. Except in the case of H^+-He collisions, these data are for impact energies less than 100 keV. The accuracy of the data was tested by subtracting the appropriate charge-transfer cross section from the total multiple-ionization cross section and comparing with measured values of σ_q^{11}.

As stated, these measured direct multiple-ionization cross sections contain contributions from direct multiple outer-shell ionization and from direct ionization of an inner-shell electron followed by Auger relaxation processes. Hence cross sections for direct multiple outer-shell ionization were deduced from the σ_q^{11} data in the following manner. At low impact energies where inner-shell ionization is negligible, σ_q^{11} is only due to multiple outer-shell ionization. To obtain the cross section for multiple outer-shell ionization for higher impact energies, where, as noted, measurements of σ_q^{11} are not available, the appropriate charge-transfer and inner-shell contributions were subtracted from the total multiple-ionization cross section (σ_q^T). This, of course, limits the accuracy of the direct multiple outer-shell ionization cross sections that we obtain to the accuracies of the individual cross sections used in the subtraction process.

The direct multiple outer-shell ionization cross sections can be used to provide information about the interaction process responsible for direct multiple ionization of atoms. For example, a direct multiple-ionization process can be thought of as proceeding in two distinct ways.[1] The incident projectile can interact with a single target electron and this electron can, in turn, interact with other target electrons so that all are ejected. This "single-step" process is clearly first order in the interaction of the projectile with the target. On the other hand, the projectile can interact with a target electron and then with a second target electron, etc., ejecting each of them. This "multistep" process is, of course, qth order in interaction of the projectile with the target corresponding to the qth term of a perturbation expansion.

The importance of the distinction between a first- and a higher-order process lies in the fact that the incident energy dependence of the cross section differs markedly between them. Roughly speaking, multiple ionization occurring via the first-order single-step process will have the same energy dependence as the single-ionization cross section, while multiple ionization occurring via a qth-order "multistep" process will behave as the qth power of the single-ionization cross section. The result is that the first-order single-step process will dominate at high impact energies. Thus by scrutinizing direct multiple-ionization cross sections and their ratios to single-ionization cross sections, we can infer important information as to which of the above processes is dominant or, in other words, which term in a perturbation expansion is important in describing target ionization.

Generally, then, the matrix element for direct multiple outer-shell ionization will include a number of terms. Since the cross section is the square of the matrix element a myriad of possibilities for cancellation or enhancement exist when more than a single term in the perturbation expansion is of consequence. Nevertheless, under certain circumstances, it may be possible to experimentally look at the single-step and multistep terms individually. For example, within a Born formulation the single-step term's contribution to the direct outer-shell multiple-ionization cross section is, to an excellent approximation, $a^{q-1}\sigma_V^{11}$, where a is the square of an energy-independent overlap integral and V refers to the outer valence shell. Thus, where this term dominates, $\sigma_{Vq}^{11}/\sigma_V^{11}$ is energy independent. It is essential to emphasize that these single- and multiple-ionization cross sections must be for a single shell only. Hence contributions from inner-shell ionization leading to multiple target ionization need to be separated from the outer-shell contributions.

Where the multistep term dominates, the situation is completely different. If we assume an independent-particle basis, the binary-encounter approach to the ionization of q electrons from a shell containing N electrons yields[2]

$$\sigma_{Vq}^{11}=2\pi\int_0^\infty \binom{N}{q} P(b)^q[1-P(b)]^{N-q}b\,db\ , \tag{6}$$

where b is the impact parameter, $\binom{N}{q}$ the binomial coefficient, and $1\gg P(b)=P(0)e^{-b/R}$, i.e., the ionization probability is assumed to fall off with a characteristic distance R. With these assumptions,

$$\sigma_{Vq}^{11}=\frac{2\pi R^2}{q^2}\frac{N!}{q!(N-q)!}P(0)^q\sim(\sigma_V^{11})^q\ . \tag{7}$$

Thus, where the multistep term is dominant, $(\sigma_V^{11})^q/\sigma_{Vq}^{11}$ is impact energy independent, a result that can also be obtained from general considerations. The energy dependence of σ_{Vq}^{11} will thus lie between $(\sigma_V^{11})^q$ and σ_V^{11} and will tend toward the latter at high energies. This will be true as long as terms in the perturbation series of higher order than the multistep term are unimportant which should be true for all but the smallest impact energies presented here.

In order to determine whether a multistep interaction is of importance, we can solve Eq. (7) for R in terms of σ_{Vq}^{11} and σ_V^{11};

$$R=\left[\frac{2\pi}{q^2}\frac{1}{(2\pi N)^q}\frac{N!}{q!(N-q)!}\frac{(\sigma_V^{11})^q}{\sigma_{Vq}^{11}}\right]^{1/(2q-2)}\ . \tag{8}$$

This R is seen to be proportional to $(\sigma_V^{11})^q/\sigma_{Vq}^{11}$ which should be energy independent if the multistep term dominates. Furthermore, R should approximate the size of the shell if the binary-encounter analysis is to have physical meaning.

The following section will present and analyze data leading to multiple ionization of helium, neon, argon, and krypton. Cross sections accounting for almost 100% of the total target ionization will be presented for proton impact energies ranging from 10 to 4000 keV. Following the presentation and analysis of the data for these gases, some concluding remarks will be made.

II. RESULTS AND DISCUSSION

A. Helium

The simplest atomic target where multiple ionization is possible is helium. This is also the easiest case to analyze since (a) only single or double ionization can occur, (b) no inner-shell processes with their subsequent relaxations are possible, and (c) there have been numerous experimental investigations of proton-helium collisions. All pathways leading to ionization of helium are listed in Table I. Note that autoionization is not explicitly separated but is included in either the direct-ionization or charge-transfer categories since the experiments only observed the charge states of the collision partners. This will also be the case for the other targets that will be discussed in this paper.

In Table I, the various fundamental processes (σ_K^{ij} and $\sigma_{K^2}^{ij}$) are listed vertically on the left, while the various measurable cross sections (σ_q^{ij}) are listed horizontally. The matrix, which is very simple for the case of helium, gives the relationship of the measurable to the fundamental cross sections. Thus direct double ionization of helium corresponds to double K-shell ionization ($\sigma_2^{11}=\sigma_{K^2}^{11}$) and

TABLE I. Table showing how single ($q=1$) and double ($q=2$) ionization of helium are related to the fundamental (initial vacancy) cross sections (σ_K^{ij}) and to the measurable (final target ionization charge state) cross sections (σ_q^{ij}). Here i and j are the projectile precollision and post-collision charge states. The relationship between the fundamental and measurable cross sections is to be read as a matrix as is described in the text.

q	i	j	Initial vacancy	Subsequent processes	σ_q^T	σ_q^{11}	σ_q^{10}	σ_q^{1-1}
+1	1	1			1	1		
			K					
	1	0			1		1	
+2	1	1			1	1		
	1	0	K^2		1		1	
	1	−1			1			1

single ionization occurs via direct K-shell ionization or via K-shell capture ($\sigma_1^T=\sigma_K^{11}+\sigma_K^{10}$). Likewise, double ionization occurs via direct double K-shell ionization, via K-shell capture plus K-shell ionization, or via double K capture, e.g., $\sigma_2^T=\sigma_2^{11}+\sigma_2^{10}+\sigma_2^{1-1}=\sigma_{K^2}^{11}+\sigma_{k^2}^{10}+\sigma_K^{1-1}$. Here, since helium has only K electrons, it is possible to use the fundamental and measurable notations interchangeably.

As mentioned, considerable experimental data exist for H^+-He collisions; in fact, *all* of the ionization channels listed in Table I have been investigated. Figure 1 presents absolute cross sections for each of these channels for proton impact energies between 10 and 5000 keV. A complete listing of the data references used to obtain the various cross-section curves is given in Table II. The experimental studies that did not measure absolute cross sections for the single- and double-ionization channels but rather ratios of double to single ionization were placed on an absolute scale by normalizing to total positive target ion production cross sections (σ_+) or total charge-transfer cross sections (σ^{10}) as designated in Table II. Because of the relatively small amount of double ionization that occurs and due to the fundamental interest in helium, we have shown the results of the individual measurements and, where appropriate, a "best fit" curve drawn through the composite set of data points for the various double-ionization channels.

As can be seen in Fig. 1(a), the total ionization cross sections (σ_+) of helium (by this we mean the production of target ionization which, of course, differs from the production of free electrons) is effectively dominated by single-ionization events. These single-ionization events occur via the direct ionization channel (σ_1^{11}) above approximately 100 keV and are predominately due to pure single capture (σ_1^{10}) at lower energies. Subtracting the charge-transfer cross section from the total single-ionization cross section ($\sigma_1^T-\sigma_1^{10}$) gives a result (dotted curve) which is entirely consistent with measurements of the direct single-ionization cross section (σ_1^{11}).[13,14]

Double ionization of helium [Fig. 1(b)] is less well characterized primarily because of the relatively small amount of double ionization that occurs. The charge-transfer (σ_2^{10} and σ_2^{1-1}) and direct ionization (σ_2^{11}) channels are well characterized by several independent measurements. This is also true for the higher-energy total double-ionization cross section (σ_2^T) where all the data except that of DuBois, Toburen, and Rudd[6] are in agreement. Note that σ_2^T is the sum of σ_2^{11}, σ_2^{10}, and σ_2^{1-1} by definition [Eq. (1)]. The measured σ_2^T is entirely consistent with the sum of the individually measured σ_2^{ij} cross sections above 100 keV. However, below 100 keV the data are inconsistent in that the sum exceeds σ_2^T in the 50-keV range (around the maximum in σ_2^T), while the sum is smaller than σ_2^T below 20 keV. Owing to the availability of data for the σ_2^{ij} from various groups, it is felt that the sum is more reliable than the directly measured σ_2^T cross sections in the 50-keV region. Below 20 keV the situation is less clear, but we believe the sum to be more reliable here as well. In conclusion, all channels leading to ionization of helium are well known except for those leading to double ionization for impact energies below 100 keV where inconsistencies exist.

The higher-energy capture cross sections (σ_1^{10}, σ_2^{10}, and σ_2^{1-1}) all have energy dependencies of approximately E^{-4}. These dependencies are slightly smaller than the asymptotic $E^{-11/2}$ and E^{-6} energy dependencies predicted by first and second Born theories, respectively. In the case of direct single ionization (σ_1^{11}) the energy dependence approaches $\ln E/E$ at high energies as predicted by

TABLE II. Sources of the data used in Fig. 1 to describe proton impact ionization of helium.

Cross section	Source	Comment	
σ_+	Rudd *et al.*[a]	*A* (absolute)	5—4000 keV
σ^{10}	Barnett *et al.*[b]	*C* (compilation)	0.2—10 000
	Nakai *et al.*[c]	*C* (compilation)	0.1—5000
σ_q^T	DuBois, Toburen, and Rudd[d]	*A* (absolute)	10—750
	Solov'ev *et al.*[e]	*A*	10—180
	Wexler[f]	*A*	800—3750
	Puckett and Martin[g]	*A*	150—1000
	Knudsen *et al.*[h]	*A*	1440—5000
σ_q^{10}	This work	*A*	15—100
	Horsdal-Pedersen and Larsen[i]	*N* (normalized)	40—400
	Schuch[j]	*N*	50—140
	Afrosimov *et al.*[k]	*A*	5—50
	Shah and Gilbody[l]	*A*	80—800
σ_q^{11}	Afrosimov *et al.*[k]	*A*	5—50
	Shah and Gilbody[l]	*A*	64—2380
σ_q^{1-1}	Barnett *et al.*[b]	*C*	1—200

[a]Reference 3.
[b]Reference 4.
[c]Reference 5.
[d]Reference 6.
[e]Reference 7.
[f]Reference 8.
[g]Reference 9.
[h]Reference 10.
[i]Reference 11.
[j]Reference 12.
[k]Reference 13.
[l]Reference 14.

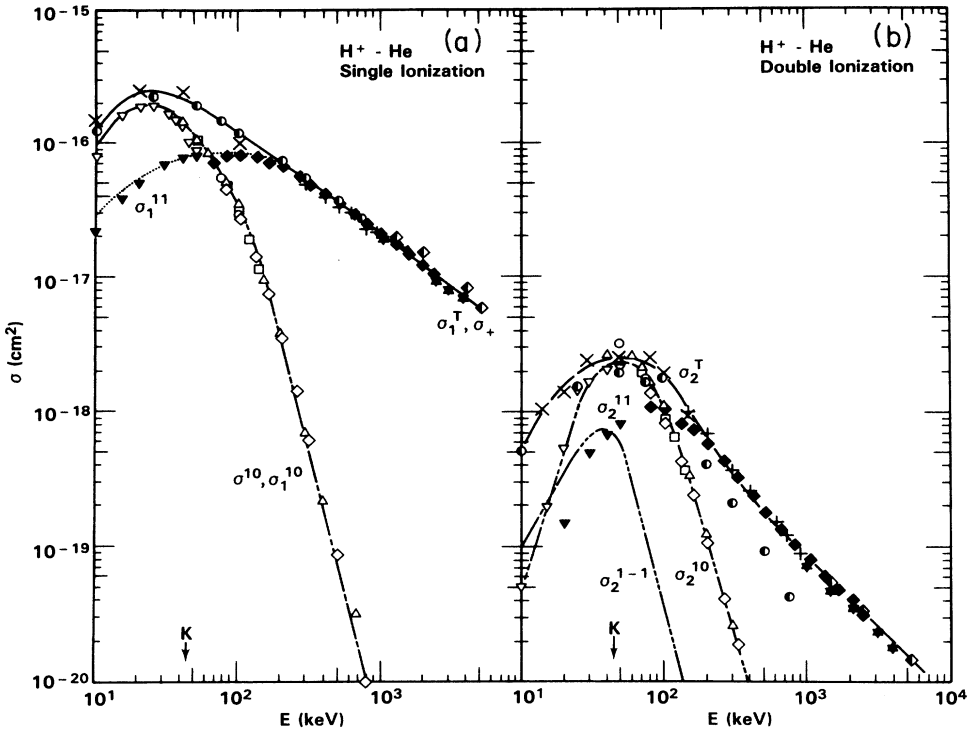

FIG. 1. Cross sections for proton impact ionization of helium. (a) Total and single ionization. σ_+: ——, Ref. 3. σ^{10}: —·—, Refs. 4 and 5. σ_1^T: ◐, Ref. 6; ×, Ref. 7; ★, Ref. 8; +, Ref. 9; ◆, Ref. 10. σ_1^{10}: ○, present work; △, Ref. 11; □, Ref. 12; ▽, Ref. 13; ◇, Ref. 14. $\sigma_1^{11} \equiv \sigma_K^{11}$: ▼, Ref. 13; ◆, Ref. 14; · · · ·, from $\sigma_1^T - \sigma_1^{10}$. (b) Double ionization. σ_2^T: ——, best fit curve to ◐, Ref. 6; ×, Ref. 7; ★, Ref. 8; +, Ref. 9; ◆, Ref. 10. σ_2^{10}: —··—, best fit curve to ○, present work; △, Ref. 11; □, Ref. 12; ▽, Ref. 13, ◇, Ref. 14. $\sigma_2^{11} \equiv \sigma_{K^2}^{11}$: ▼, Ref. 13; ◆, Ref. 14. σ_2^{1-1}: — ··· —, Ref. 4. Cross-section nomenclature is defined in the text. Proton velocity matching that of the bound target electron is indicated by the arrow.

theory.

Using the cross sections leading to single and double ionization of helium that we have presented in Fig. 1, it is possible to gain knowledge about the fundamental mechanisms leading to multiple ionization of atoms. As discussed above, when a multistep interaction mechanism dominates, R, the "interaction" distance which is proportional to $(\sigma_K^{11})^2/\sigma_{K^2}^{11}$, is a constant whereas when the single-step mechanism dominates $\sigma_{K^2}^{11}/\sigma_K^{11}$ is a constant. These ratios have been determined and the results for double ionization of He are shown in Fig. 2. An approximately constant value of R between 50 and 500 keV is seen. This indicates that the multistep term dominates in this energy region. The value of R is within a factor of 2 of the Hartree-Fock value of $\langle r \rangle$ for the K shell of He,[15] which is not unreasonable.

Above 500 keV, R is no longer constant, indicating that the multistep term is no longer the only important term in a perturbation expansion. To explore this further, the ratio $\sigma_{K^2}^{11}/\sigma_K^{11}$ is also shown in Fig. 2 at the higher impact energies. This ratio is clearly energy dependent but appears to be flattening out at the highest impact energies. This indicates the emerging dominance of the single-step term in the perturbation series. Taken as a whole, then, Fig. 2 suggests that between 50 and 500 keV impact energies, only the multistep term need be considered, from 500 to 5000 keV *both* terms must be considered, and above 5000 keV, only the single-step term is required.

B. Neon

Following the procedure that has been outlined for helium, we now turn our attention to a somewhat more com-

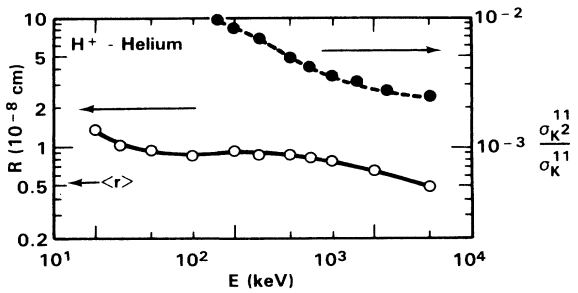

FIG. 2. Ratios of direct double ($\sigma_{K^2}^{11}$) to single (σ_K^{11}) K-shell ionization cross sections for H^+-He collisions used to determine the multiple-ionization mechanism. Multistep mechanism: ○, using left-hand scale with R as defined by Eq. 8 in text. Single-step mechanism: ●, using right-hand scale. The curves serve only to guide the eye. The helium $1s$ Hartree-Fock value $\langle r \rangle$ is indicated by the arrow.

plex target neon. Table III lists the various channels leading to single, double, and triple ionization of neon. The table is in the same form as Table I for helium, with one major exception. Neon has an inner shell and when an electron is removed from the inner shell, the vacancy can decay in a variety of ways which can lead to different charge states. Thus, after the initial production of inner-shell vacancies, there are branching ratios for the various subsequent processes. Where the branching ratio is quite close to unity, it has been set equal to one in Table III. This is seen in the case of the KLL Auger decay following an initial K-shell or KL vacancy. In the case of triple ionization, we see from Table III that $\sigma_3^{11}=\sigma_{L^3}^{11}+\sigma_{KL}^{11}+a\sigma_K^{11}$, where a is the fraction of K vacancies undergoing $KLLL$ double Auger decay.

Single ionization of neon occurs only via L-shell vacancy production. This can be a result of direct L-shell ionization (σ_L^{11}) or via L-shell capture (σ_L^{10}). Table III shows that these are related to the measurable quantities by $\sigma_L^{11}=\sigma_1^{11}$ and $\sigma_L^{10}=\sigma_1^{10}$. On the other hand, double ionization can result from the production of two L-shell vacancies or from an initial K-shell vacancy followed by a KLL Auger relaxation. Double L-shell vacancies result from direct double ionization ($\sigma_{L^2}^{11}$), single capture plus one additional ionization ($\sigma_{L^2}^{10}$), or double capture events ($\sigma_{L^2}^{1-1}$); single K vacancies result from direct ionization (σ_K^{11}) or capture (σ_K^{10}) of a K-shell electron.

Triple ionization occurs via ionization and capture of three L-shell electrons or via K-shell ionization followed by Auger relaxation. The K-shell ionization can be accomplished by L-shell ionization, either in the initial or in the relaxation stage, via shakeoff plus KLL Auger emission or via double Auger emission ($KLLL$ Auger).

Experiments where only the initial and final charge states of the collision partners are measured cannot distinguish double L-shell ionization from K-shell ionization followed by an Auger relaxation in either the direct (σ_1^{11}) or single capture (σ_2^{10}) cross-section channels. However, it is necessary to separate the direct double-ionization contributions resulting from outer- and inner-shell ionization in order to evaluate whether a multistep or single-step outer-shell ionization mechanism is important. Information about the inner-shell contribution to double ionization cannot be determined from total K-shell vacancy production cross sections ($\sigma_K^T=\sigma_{KL^0}^T+\sigma_{KL}^T+\cdots$) alone; spectroscopic information is also required. This is because inner-shell ionization is often accompanied by, or results in outer-shell ionization either during the initial interaction or via subsequent Auger cascading processes. In both cases, inner-shell vacancies lead to higher degrees of target ionization than occurs for a single inner-shell vacancy followed by a single simple Auger relaxation. Information about which of these processes occurs is available through high-resolution spectroscopy from which branching ration information about the inner-shell relaxation channels is obtained. Studies of resultant target ionization charge-state distributions resulting from inner shell ionization can also yield branching ratio information.

Cross sections leading to the first three ionization states of neon are shown in Fig. 3 and their sources are listed in Table IV. Except for direct ionization (σ_q^{11}), curves are shown that represent the data for the various ionization channels. This is because only a single set of data exists for certain channels or else the various experimental investigations are in relatively good agreement with each other. It is also done to enhance the "readability" of the

TABLE III. Table showing how single, double, and triple ($q=1-3$) ionization of neon are related to initial vacancy production cross sections and to measurable final target ionization state cross sections. The relationship between the initial vacancy and the final charge-state cross sections is to be read as a matrix. a is the fraction of K vacancies undergoing $KLLL$ Auger decay.

q	i	j	Initial vacancy	Subsequent processes	σ_q^T	σ_q^{11}	σ_q^{10}	σ_q^{1-1}
+1	1	1			1	1		
			L					
	1	0			1		1	
+2	1	1			1	1		
	1	0	L^2		1		1	
	1	−1			1			1
	1	1			1	1		
	1	0	K	KLL Auger	1		1	
+3	1	1			1	1		
	1	0	L^3		1		1	
	1	−1			1			1
	1	1			1	1		
	1	0	KL	KLL Auger	1		1	
	1	−1			1			1
	1	1			a	a		
	1	0	K	$KLLL$ Auger	a		a	

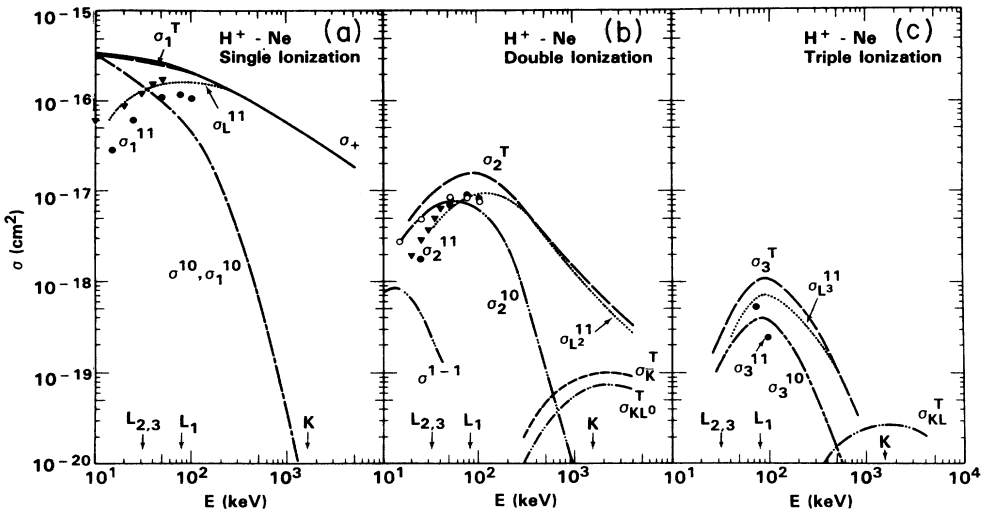

FIG. 3. Cross sections for proton impact ionization of neon. (a) Total and single ionization. σ_+: ——, Ref. 3. σ^{10}: —·—, Refs. 4 and 5. σ_1^T: ——, Ref. 6. σ_1^{10}: —·—, Refs. 11–13 and 16. σ_1^{11}: ▼, Ref. 13; ●, Ref. 16. σ_L^{11}: · · · ·, from $\sigma_1^T-\sigma_1^{10}$. (b) Double ionization. σ_2^T: ——, Ref. 6. σ_2^{10}: —··—, Refs. 11–13 and 16. σ^{1-1}: — · · · —, Ref. 4. σ_K^T: — — —, Refs. 17–19. $\sigma_{KL^0}^T$: —··—, σ_K^T combined with Refs. 20–23. σ_2^{11}: ▼, Ref. 13; ●, Ref. 16. $\sigma_{L^2}^{11}$: · · · ·, $\sigma_2^T-\sigma_2^{10}-\sigma_{KL^0}^T$. (c) Triple ionization. σ_3^T: ——, Ref. 6. σ_3^{10}: —··—, Refs. 11–13 and 16. σ_{KL}^T: — · · —, σ_K^T combined with Refs. 20–23. σ_3^{11}: ●, Ref. 16. $\sigma_{L^3}^{11}$: · · · ·, $\sigma_3^T-\sigma_3^{10}-\sigma_{KL}^T$. Cross-section nomenclature is defined in the text. Proton velocities matching those of the bound electrons are indicated by the arrows.

figure. As was done for helium, relative measurements have been placed on an absolute scale by normalizing to the appropriate total cross sections.

The total ionization cross section (σ_+) of neon [Fig. 3(a)] is essentially due to single-ionization events with double ionization at least an order of magnitude less likely, just as for helium. Of the contributions to single ionization, direct single ionization of neon (σ_1^{11}), i.e., L-shell ionization (σ_L^{11}), dominates above 100 keV with L-shell capture (σ_L^{10}) being dominant at lower impact energies. Subtracting the charge transfer channel from the total single-ionization cross section yields the dotted curve which is consistent with the direct ionization measurements (σ_1^{11}) of Afrosimov *et al.*[13] The σ_1^{11} measurements of DuBois,[16] although having the proper energy dependence, are approximately 50% smaller.

Double ionization of neon [Fig. 3(b)] is almost entirely due to double L-shell vacancy production with K-shell ionization playing a minor role even at the highest energies shown. It is somewhat surprising that double L-shell ionization should be far more likely than *single* K-shell ionization. But, as noted previously,[17,24] this is an inescapable conclusion of the analysis. Physically, this can be understood by noting that the "area" ($\pi\langle r\rangle^2$) of the L shell is almost three orders of magnitude larger than the K shell and, thus, σ_L^{11} is correspondingly larger than σ_K^{11}. Hence, even though $\sigma_{L^2}^{11}$ is only a small fraction of σ_L^{11} ($\sim 1\%$), it is still large compared to σ_K^{11}. Where the size of an inner shell is not so small compared to the outer shell, as for example in krypton, a rather different phenomenology should result. This will be shown later.

Double ionization of neon at higher impact energies results from direct double ionization (σ_2^{11}) with the charge transfer plus ionization channel (σ_2^{10}) becoming dominant only below 50 keV. The double capture channel (σ_2^{1-1}) can be neglected except perhaps for very low impact energies. Energy dependences for σ_1^{10} and σ_2^{10} are approximately $E^{-4.8}$ and $E^{-3.8}$, respectively, and the energy dependence of σ_1^{11} is slightly less than the $\ln E/E$ dependence predicted by theory.

Since σ_2^{1-1} is negligible, subtracting the charge-transfer channel (σ_2^{10}) from the total double-ionization cross section (σ_2^T) should give σ_2^{11}. At lower energies this is due to double L-shell ionization ($\sigma_{L^2}^{11}$) but for higher energies the inner-shell contribution must also be subtracted to provide information about the direct double L-shell ionization cross section. This result (dotted curve) shows good agreement with the σ_2^{11} measurements of Afrosimov *et al.*[13] and DuBois[16] below 100 keV. Note that at higher energies it is the cross section for K-shell ionization with *no* additional L-shell ionization ($\sigma_{KL^0}^T$) that was subtracted. This was obtained by combining the total K-shell cross section (σ_K^T with spectroscopic information[20–22] where satellite lines resulting from initial KL and KL^2 vacancies were identified and their intensities established with respect to lines resulting from initial KL^0 vacancies. (Here we have explicitly written that no L-shell ionization accompanies the K-shell ionization. This notation is entirely equivalent to σ_K^T which follows the initial vacancy notation of Table III.) As can be seen, $\sigma_{KL^0}^T$ is approximately 25% smaller than the total K-shell cross section (σ_K^T). Since the K-shell capture cross sections ($\sigma_{KL^0}^{10}$) are small relative to the total K-shell ionization cross sections,[18] they do not appear in Fig. 3(b). Thus, to an excellent approximation, $\sigma_{KL^0}^T=\sigma_{KL^0}^{11}$.

TABLE IV. Sources of the data used in Fig. 3 to describe proton impact ionization of neon.

Cross section	Source	Comment	
σ_+	Rudd *et al.*[a]	*A* (absolute)	5–4000 keV
σ^{10}	Barnett *et al.*[b]	*C* (compilation)	0.4–4000
	Nakai *et al.*[c]	*C*	0.1–4370
σ_q^T	DuBois, Toburen, and Rudd[d]	*A*	10–4000
σ_q^{10}	Horsdal-Pedersen and Larson[e]	*N* (normalized)	50–2000
	Schuch[f]	*N*	30–120
	Afrosimov *et al.*[g]	*A*	5–50
	DuBois[h]	*A*	15–100
σ_q^{11}	Afrosimov *et al.*[g]	*A*	5–50
	DuBois[h]	*A*	15–100
σ^{1-1}	Barnett *et al.*[b]	*C*	2–40
σ_2^{1-1}	Afrosimov *et al.*[g]	*A*	15–50
σ_K^T	Manson, DuBois, and Toburen[i]	*A* (Auger)	300–3670
	Rødbro *et al.*[j]	*A* (Auger)	300–1500
	Stolterfoht and Schneider[k]	*A* (Auger)	100–600
$\sigma_{KL^i}^T$	Stolterfoht, Gabler, and Leithäuser[l]	*N* (from Auger spectroscopy)	4200
	Edwards and Rudd[m]	*N* (from Auger spectroscopy)	300
	Krause *et al.*[n]	*N* (from Auger spectroscopy)	3.2[p]
	Carlson and Krause[o]	*N* (from charge state ratios)	0.93–17.5[q]
$\sigma_{KL^0}^{10}$	Rødbro *et al.*[j]	*A* (Auger)	400–1500

[a]Reference 3.
[b]Reference 4.
[c]Reference 5.
[d]Reference 6.
[e]Reference 11.
[f]Reference 12.
[g]Reference 13.
[h]Reference 16.
[i]Reference 17.
[j]Reference 18.
[k]Reference 19.
[l]Reference 20.
[m]Reference 21.
[n]Reference 22.
[o]Reference 23.
[p]For electron impact.
[q]For x-ray impact.

Triple ionization of neon can occur via triple L ionization, KL ionization followed by a KLL Auger transition, or by K-shell ionization followed by a $KLLL$ double Auger transition (see Table III). The available experimental cross-section information for triple ionization is shown in Fig. 3(c). Due to the limited amount of data available, little can be said. We have, however, obtained the direct triple-ionization cross section at lower energies by subtraction ($\sigma_3^{11}=\sigma_3^T-\sigma_3^{10}$). σ_3^{1-1} is considered to be negligible with respect to σ_3^T since the σ_2^{1-1} measurements of Afrosimov *et al.*[13] are approximately equal to the total σ^{1-1} cross sections. At these low impact energies there is no appreciable inner-shell contribution so σ_3^{11} is equal to the cross section for direct triple L-shell ionization ($\sigma_{L^3}^{11}$). This [the dotted curve in Fig. 3(c)] is compared to the only experimental data available[16] and is in reasonable agreement since the experimental σ_3^{11} cross sections are subject to large uncertainties. Thus specific conclusions cannot be drawn about overall consistency of the data. For impact energies above 1 MeV, data for σ_3^T do not exist and thus cannot be compared to the σ_{KL}^T cross section shown in Fig. 3(c).

In summary then, sufficient data now exist to characterize single and double ionization of neon by proton impact. Triple ionization requires additional information, namely total triple-ionization cross sections (σ_3^T) at high impact energies and more accurate direct triple-ionization cross sections (σ_3^{11}). Furthermore, little information about possible double Auger transitions[25] is available. Although double Auger processes are less probable than single Auger processes, they can form an important contribution to higher ionization states, as will be shown for heavier targets.

The interaction distance R obtained using the direct L, L^2, and L^3 ionization cross sections (dotted curves in Fig. 3) is shown in Fig. 4. The fact that R, which is proportional to $(\sigma_L^{11})^q/\sigma_{L^q}^{11}$ is roughly constant in the 100–1000-keV region argues for the dominance of the multistep term in the perturbation expansion in this energy range. Identical values for R obtained using the double- and triple-ionization data makes this case still stronger, and also indicates that the $\sigma_{L^3}^{11}$ cross sections shown in Fig. 3(c) (dotted curve) are more accurate than are the σ_3^{11} measurements. It would, thus, seem reasonable to assume that the same constant value of R should apply for all states of ionization in this energy range. If so, $\sigma_{L^q}^{11}$ could be obtained for $q=4$–8 by using Eq. (7).

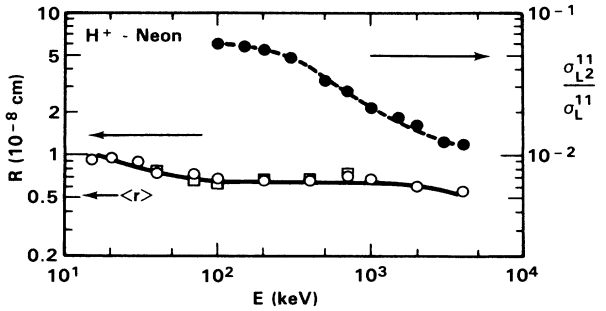

FIG. 4. Ratios of direct multiple to single outer-shell ionization cross sections for H^+-Ne collisions used to determine the multiple-ionization mechanisms. Multistep mechanism: ○ (double ionization) and □ (triple ionization) using the left-hand scale. R is defined by Eq. (8). Single-step mechanism: ● and right-hand scale. The curves serve only to guide the eye. The Hartree-Fock value for the neon $2p$ electron $\langle r \rangle$ is indicated by the arrow.

The energy range over which R is constant for neon is roughly the same as for helium. Likewise, the value of R obtained is similarly related to the Hartree-Fock value[15] $\langle r \rangle$. In addition, at the higher energies, R falls off just as in helium. Here the ratio $\sigma_{L^2}^{11}/\sigma_L^{11}$ (also shown in Fig. 4) shows evidence of becoming constant above 4000 keV, indicating that the single-step term is becoming the most important. Thus, helium and neon behave in the same manner with respect to which mechanisms contribute and where they are the most important.

C. Argon

Multiple ionization of argon is more complicated than that of neon because of the increasing number of inner-shell relaxation modes available. Table V lists the major ionization channels leading to single, double, and triple ionization of argon. Including the possibility of four times ionized argon would roughly double the size of the table. As can be seen in Table V, we have now divided the L-shell ionization into its components, namely $2s$ and $2p$ ionization owing to the possibility of Coster-Kronig transitions. However, in general, insufficient data exist to provide $2s$ and $2p$ subshell cross-section information. Observe that information about the branching ratios in the relaxation channels becomes very important; thus a significant number of the coefficients in the table are seen to differ from unity.

Figure 5 presents cross sections for single and multiple ionization of argon for proton energies between 10 and 4000 keV compiled from the sources listed in Table VI. As can be seen, multiple ionization is responsible for 20—50 % of the total ionization cross section (σ_+), in contrast to He and Ne where the single-ionization process is responsible for almost all of the total ionization. Also note that the total charge-transfer cross section (σ^{10}) changes slope when the proton velocity is approximately the same as the bound L-shell electron velocity. This is an indication of capture from the L shell becoming important. The L-shell capture cross section [σ_L^{10} in Fig. 5(a)] has been directly measured[18] and is seen to be in excellent agreement with the higher-energy total single capture cross section (σ^{10}). Therefore in this region neither the K shell nor the M shell contribute appreciably to the capture cross section.

Pure single capture (σ_1^{10}), i.e., capture of an M-shell electron represents most of the total capture cross section for energies less than 200 keV with L-shell capture becoming an increasingly more important component of σ^{10} at higher energies. The energy dependence of σ_1^{10} is approximately $E^{-4.8}$ for energies between 150 and 400 keV with a slower dependence of $E^{-3.1}$ for higher energies. One possible explanation for this change in slope for proton velocities near that of the bound L-shell electron velocities is capture of an L-shell electron followed by x-ray decay. Thus the increased σ_1^{10} cross section above approximately 500 keV could be due to x-ray decay of an L-shell vacancy. But this would require an argon L-shell fluorescence yield of several percent which is an order of magnitude larger than the currently accepted value.[31] Thus this change in slope is, as yet, unexplained.

By subtracting the M-shell capture from the total single-ionization cross section (σ_1^T), the cross section for direct ionization on one M-shell electron (σ_M^{11}) can be obtained. This (the dotted curve) is seen to be in excellent agreement with new measurements of σ_1^{11} presented here whereas the σ_1^{11} data of Afrosimov *et al.*[26] are larger at the lowest energies. At higher impact energies, σ_1^{11} has approximately the same energy dependence as was seen for neon, slightly less than $\ln E/E$.

Figure 5(b) shows the individual cross sections leading to double ionization of argon and the total double-ionization cross section. It is seen that the capture plus ionization channel (σ_2^{10}) is the primary mechanism for producing doubly ionized argon for impact energies less than 50 keV; inner-shell ionization dominates above 700 keV and is, in fact, virtually *totally* responsible for double ionization above 2 MeV. Only between 50 and 700 keV does direct double outer-shell ionization ($\sigma_{M^2}^{11}$) dominate (dotted curve). Note that this is rather different than neon where direct double outer-shell ionization still dominated over single inner-shell ionization in the MeV region. Double capture and K-shell ionization are entirely negligible for the energy range shown.

As was noted in the case of neon, it is essential to have spectroscopic information about the inner-shell ionization channel since inner-shell ionization can be accompanied with simultaneous outer-shell ionization, e.g., $\sigma_L^T = \sigma_{LM^0}^T + \sigma_{LM}^T + \sigma_{LM^2}^T + \cdots$. The importance of this is clear in Fig. 5(b) where the total measured L-shell cross section (σ_L^T) is observed to be considerably larger than the total measured double-ionization cross section (σ_2^T) above 1 MeV.

In order to determine the $\sigma_{LM^n}^{ij}$ cross sections that lead to double or higher degrees of ionization, inner-shell relaxation branching ratio information obtained from high-resolution spectroscopic studies[27,28] is required. It is also possible to determine these branching ratios from charge state information where inner-shell vacancy production is known to dominate.[11,29,30] In determining the branching

TABLE V. Table showing how single, double, and triple ($q=1-3$) ionization of argon are related to initial vacancy production cross sections and to measurable final target ionization state cross sections. The relationship between the initial vacancy and the final charge-state cross sections is to be read as a matrix as illustrated.

q	i	j	Initial vacancy	Subsequent processes	σ_q^T	σ_q^{11}	σ_q^{10}	σ_q^{1-1}
+1	1	1			1	1		
	1	0	M		1		1	
+2	1	1			1	1		
	1	0	M^2		1		1	
	1	−1			1			1
	1	1	$2p$	$2pMM$ Auger	a	a		
	1	0			a		a	
	1	1	$2s$	$2sMM$ Auger	b	b		
	1	0			b		b	
	1	1	K	KMM Auger	c	c		
	1	0			c		c	
+3	1	1			1	1		
	1	0	M^3		1		1	
	1	−1			1			1
	1	1			d	d		
	1	0	$2pM$	$2pMM$ Auger	d		d	
	1	−1			d			d
	1	1			e	e		
	1	0	$2sM$	$2sMM$ Auger	e		e	
	1	−1			e			e
	1	1			f	f		
	1	0	KM	KMM Auger	f		f	
	1	−1			f			f
	1	1	$2p$	$2pMMM$ Auger	g	g		
	1	0			g		g	
	1	1	$2s$	$2s2pM$ Coster-Kronig plus $2pMM$ Auger,	$hd+i$	$hd+i$		
	1	0		or $2sMMM$ Auger	$hd+i$		$hd+i$	
	1	1	K	$K2sM$ plus $2sMM$ Auger,	$je+kd+l$	$je+kd+l$		
	1	0		or $K2pM$ plus $2pMM$ Auger, or $KMMM$ Auger	$je+kd+l$		$je+kd+l$	

e.g., $\sigma_2^{10}=\sigma_{M^2}^{10}+a\sigma_{2p}^{10}+b\sigma_{2s}^{10}+c\sigma_K^{10}$

a is the fraction of $2p$ vacancies filled by $2pMM$ Auger

b is the fraction of $2s$ vacancies filled by $2sMM$

c is the fraction of K vacancies filled by KMM

d is the fraction of $2pM$ vacancies filled by $2pMM$

e is the fraction of $2sM$ vacancies filled by $2sMM$

f is the fraction of KM vacancies filled by KMM

g is the fraction of $2p$ vacancies filled by $2pMMM$

h is the fraction of $2s$ vacancies filled by $2s2pM$ Coster-Kronig

i is the fraction of $2s$ vacancies filled by $2sMMM$ Auger

j is the fraction of K vacancies filled by $K2sM$

k is the fraction of K vacancies filled by $K2pM$

l is the fraction of K vacancies filled by $KMMM$

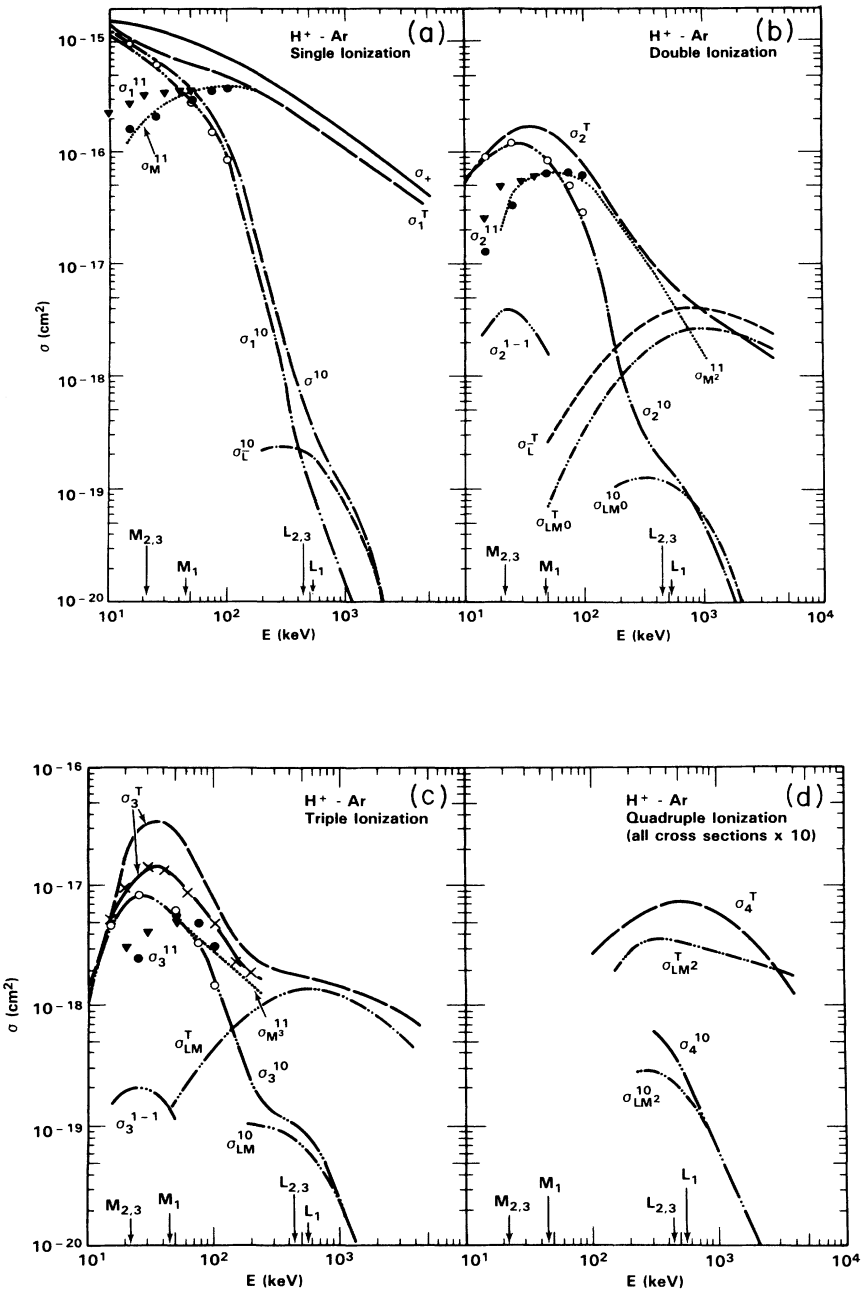

FIG. 5. Cross sections for proton impact ionization of argon. (a) Total and single ionization. σ_+: ——, Ref. 3. σ^{10}: —·—, Refs. 4 and 5. σ_1^T: ——, Ref. 6. σ_L^{10}: —·—, Ref. 18. σ_1^{10}: ○, present work; —··—, Refs. 11, 12, and 26. σ_1^{11}: ●, present work; ▼, Ref. 26. σ_M^{11}: · · · ·, from $\sigma_1^T-\sigma_1^{10}$. (b) Double ionization. σ_2^T: ——, Ref. 6. σ_2^{10}: ○, present work; —··—, Refs. 11, 12, and 26. σ_2^{1-1}: — ··· —, Ref. 26. $\sigma_{LM^0}^{10}$: —··—, σ_L^{10} combined with Refs. 11 and 27–30. σ_L^T: – – –, present work and Ref. 27. $\sigma_{LM^0}^T$: —··—, σ_L^T combined with Refs. 11 and 27–30. σ_2^{11}: ●, present work, ▼, Ref. 26. $\sigma_{M^2}^{11}$: · · · ·, from $\sigma_2^T-\sigma_2^{10}-\sigma_{LM^0}^T-\sigma_2^{1-1}$. (c) Triple ionization. σ_3^T: ——, Ref. 6; —×—, Ref. 7. σ_3^{10}: ○, present work; —··—, Refs. 11, 12, and 26. σ_3^{1-1}: — ··· —, Ref. 26. σ_{LM}^{10}: —··—, σ_L^{10} combined with Refs. 11 and 27–30. σ_{LM}^T: —··—, σ_L^T combined with Refs. 11 and 27–30. σ_3^{11}: ●, present work; ▼, Ref. 26. $\sigma_{M^3}^{11}$: · · · ·, from $\sigma_3^T-\sigma_3^{10}-\sigma_{LM}^T-\sigma_3^{1-1}$. (d) Quadruple ionization. σ_4^T: ——, Ref. 6. σ_4^{10}: —··—, Refs. 11, 12, and 26. $\sigma_{LM^2}^{10}$: —··—, σ_L^{10} combined with Refs. 11 and 27–30. $\sigma_{LM^2}^T$: —··—, σ_L^T combined with Refs. 11 and 27–30. Cross-section nomenclature is defined in the text. Proton velocities matching those of the bound target electrons are indicated by the arrows.

TABLE VI. Sources of the data used in Fig. 5 to describe proton impact ionization of argon.

Cross section	Source	Comment	
σ_+	Rudd *et al.*[a]	*A* (absolute)	5—4000
σ^{10}	Barnett *et al.*[b]	*C* (compilation)	0.07—40 000
	Nakai *et al.*[c]	*C*	0.1—13 800
σ_q^T	DuBois, Toburen, and Rudd[d]	*A*	10—4000
	Solov'ev *et al.*[e]	*A*	15—180
σ_q^{10}	This paper	*A*	15—100
	Horsdal-Pedersen and Larsen[f]	*N* (normalized)	50—2000
	Schuch[g]	*N*	30—120
	Afrosimov and Mamaev *et al.*[h]	*A*	5—50
σ_q^{11}	This paper	*A*	15—100
	Afrosimov and Mamaev *et al.*[h]	*A*	5—50
σ_q^{1-1}	Afrosimov and Mamaev *et al.*[h]	*A*	15—50
σ_L^T	Stolterfoht, Schneider, and Ziem[i]	*A* (Auger)	50—600
	This paper	*A* (Auger)	250—3670
$\sigma_{LM^i}^T$	Horsdal-Pedersen and Larsen[f]	*N* (charge state ratios for capture)	500—2000
	Stolterfoht, Schneider, and Ziem[i]	*N* (branching ratios from Auger)	50—600
	Oona[j]	*N* (branching ratios from x rays)	150—500
	Carlson and Krause[k]	*N* (charge state ratios)	1—17.5[n]
	Hippler, Bessler, and Lotz[l]	*N* (charge state ratios)	300
σ_L^{10}	Rødbro *et al.*[m]	*A*	200—2000
$\sigma_{LM^i}^{10}$		*N* (using branching ratios from above)	

[a]Reference 3.
[b]Reference 4.
[c]Reference 5.
[d]Reference 6.
[e]Reference 7.
[f]Reference 11.
[g]Reference 12.
[h]Reference 26.
[i]Reference 27.
[j]Reference 28.
[k]Reference 29.
[l]Reference 30.
[m]Reference 18.
[n]For x-ray impact.

ratios from charge-state information, it was observed that consistent results were obtained for experimental work where inner-shell ionization[29,30] dominated *and* for where inner-shell capture[11] dominated. The only exception was for the $\sigma_{LM^2}^T$ data of Stolterfoht *et al.*[27] which are not in agreement with the majority of the branching-ratio data. Thus the majority of the date imply that the probability of outer-shell ionization accompanying inner-shell ionization is independent of the inner-shell vacancy production mechanism. Using this observation, we can then untangle the total *L*-shell cross section (σ_L^T) into its constituents ($\sigma_{LM^n}^T$ where $n=0,1,2$) and likewise divide the total *L*-shell capture cross section (σ_L^{10}) into its constituents ($\sigma_{LM^n}^{10}$) by using the *same* branching ratios.

Doing so, the cross section for *L*-shell vacancy production with no additional *M*-shell ionization ($\sigma_{LM^0}^T$) was determined. This cross section, which is approximately equal to $\sigma_{LM^0}^{11}$ since the *L*-shell capture components are but a small part of the total *L*-shell cross section, is seen to be about 30—50% smaller than the total *L*-shell cross section in Fig. 5(b) and is in excellent agreement with the total double-ionization cross section (σ_2^T) at higher energies. Likewise, the cross section for *L*-shell *capture* with no additional *M*-shell ionization ($\sigma_{LM^0}^{10}$) was determined and is seen to be in excellent agreement with measurements of σ_2^{10} where *M*-shell capture *plus* *M*-shell ionization is not separated from *L*-shell capture followed by an Auger relaxation. Using the data for σ_2^{10} and $\sigma_{LM^0}^{10}$ it is, in principle, possible by subtraction to extend the data for $\sigma_{M^2}^{10}$ to higher energies since $\sigma_2^{10}=\sigma_{M^2}^{10}+\sigma_{LM^0}^{10}$. However, the data are not sufficiently accurate to do so meaningfully.

By subtracting the capture (σ_2^{10}) and the inner-shell ionization cross sections ($\sigma_{LM^0}^{11}$) from σ_2^T, one obtains the direct double outer-shell ionization cross section $\sigma_{M^2}^{11}$. At lower impact energies, the value obtained by subtraction (dotted curve) is in excellent agreement with the new experimental σ_2^{11} date presented here. The lower energy σ_2^{11} measurements of Afrosimov *et al.*[26] are again too large as was seen for single ionization of argon.

Cross sections leading to triple ionization of argon are shown in Fig. 5(c). Here, as was seen in the case of double ionization, the inner-shell ionization channel (σ_{LM}^T which is approximately equal to σ_{LM}^{11} since $\sigma_{LM}^{10} \ll \sigma_{LM}^T$) is virtually entirely responsible for triple ionization of argon at higher impact energies. However, the inner-shell contribution becomes dominant at lower energies than in the case of double ionization. We feel that above 500 keV σ_3^T and σ_{LM}^T agree within their combined uncertainties.

Excellent agreement between the higher energy σ_3^{10} cross sections and the *L*-shell capture cross section leading to triply ionized argon (σ_{LM}^{10}) is found. This provides

further confidence in our assumption that the same branching-ratio information can be applied to the capture channels and to the ionization channels. The lower energy capture cross section σ_3^{10} is primarily M-shell capture plus simultaneous double M-shell ionization ($\sigma_{M^3}^{10}$), since σ_{LM}^{10} is negligibly small. σ_3^{10} is seen to be considerably more likely than is double M-shell capture plus one additional M electron being simultaneously ionized, i.e., $\sigma_{M^3}^{1-1}$ which is the dominant contributor to σ_3^{1-1}.

The individual σ_3^{ij} cross sections shown do not add up to the total triple-ionization cross section (σ_3^T) taken from Ref. 6 for impact energies below approximately 200 keV. Since the σ_3^{10} and σ_3^{11} cross sections measured by different groups are in relatively good agreement, the fault is assumed to lie in the σ_3^T measurements of DuBois, Toburen, and Rudd.[6] Their cross sections are larger at low energies than those measured by Solov'ev *et al.*[7] [shown in Fig. 5(c)] which are in better, but not complete, agreement with the sum $\sigma_3^{11}+\sigma_3^{10}+\sigma_3^{1-1}$. Above 150 keV the σ_3^T data of DuBois, Toburen, and Rudd[6] and Solov'ev *et al.*[7] are in near agreement with each other and with the sum.

Due to inconsistencies in the data, we have taken the cross section for direct triple outer-shell ionization to be given by the experimental σ_3^{11} measurements for energies up to 100 keV with an extension to higher energies obtained from $\sigma_{M^3}^{11}=\sigma_3^T-\sigma_3^{10}-\sigma_3^{1-1}-\sigma_{LM}^{11}$. It is not possible to extend this cross section above 200 keV with any reliability due to uncertainties in the σ_3^T and σ_{LM}^{11} cross sections.

Although we have not included the channels leading to four-times-ionized argon in Table V, there exists some experimental information from which we can determine the dominant channels. These limited data are shown in Fig. 5(d). Considering the similar appearance between the σ_4^T and $\sigma_{LM^2}^T$ curves and the fact that inner-shell vacancy production has been shown to account for virtually all the higher energy double- and triple-ionization cross section, it is believed that $\sigma_{LM^2}^T$ should entirely account for the σ_4^T cross section. Note that the branching-ratio data used to determine $\sigma_{LM^2}^T$ excludes the high-resolution Auger spectroscopic data of Stolterfoht *et al.*[27] since these data are inconsistent with data from several other sources.[28–30] Using the same branching ratios to determine the component of L-shell capture leading to four times ionized argon ($\sigma_{LM^2}^{10}$) gives a result that is entirely consistent with the σ_4^{10} cross sections at higher energies. Finally, since $\sigma_4^{10} \ll \sigma_{LM^2}^T$, one can infer that $\sigma_{LM^2}^T \approx \sigma_{LM^2}^{11}$ over the energy range shown.

In order to test if the multistep interaction picture appropriately models direct multiple-ionization cross sections, we have again determined the interaction distance R from ratios of direct multiple to direct single outer-shell ionization using the cross sections from Fig. 5 as described. The results are shown in Fig. 6 where the values of R are seen to have approximately the same energy dependence for the double- and triple-ionization cases. It is unclear whether the energy dependence of R is due to uncertainties in the data or whether the model is inappropriate in the present case. It is apparent, though, that simply the ratio of direct double to single outer-shell ionization ($\sigma_{M^2}^{11}/\sigma_M^{11}$) is strongly energy dependent for the energy range shown. Thus the single-step approximation is totally inappropriate in this region. Further, the $\sigma_{M^2}^{11}/\sigma_M^{11}$ ratio does not seem to be flattening at the highest energy (1 MeV) for which we have data. By 4 MeV, the ratios for both helium and neon were approaching a constant value and it may be that higher energy data for argon would show the same trend. This remains an open question.

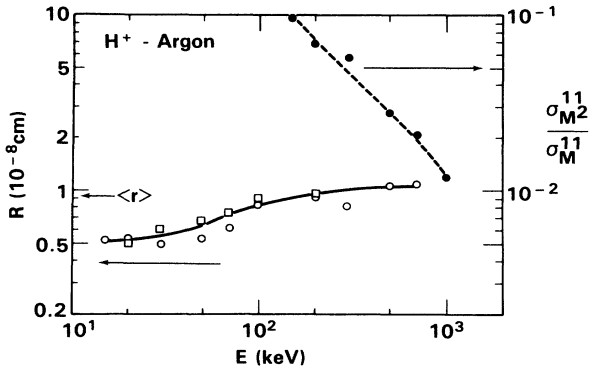

FIG. 6. Ratios of direct multiple to single outer-shell ionization cross sections for H^+-Ar collisions used to determine the multiple-ionization mechanism. Multistep mechanism: ○ (double ionization) and □ (triple ionization) used with the left-hand scale. R is defined by Eq. (8). Single-step mechanism: ●, used with the right-hand scale. The curves serve only to guide the eye. The Hartree-Fock value for the argon $3p$ electron $\langle r \rangle$ is indicated by the arrow.

In summary, we have shown that single and double ionization of argon are well characterized and that L-shell ionization followed by Auger relaxation completely dominates the multiple-ionization cross section at higher energies. The total cross section for producing triply ionized argon needs to be more accurately measured as do the cross sections leading to four times ionized argon. Because of the importance of inner-shell ionization, it is essential to have as detailed information as possible concerning cross sections and branching ratios.

D. Krypton

Krypton represents a still more formidable challenge to analyze the observed multiple ionization in terms of production mechanisms. This is because M-shell ionization leading to Auger relaxation will be shown to be of major importance for proton impact energies above 200 keV. It is readily apparent from Table VII that detailed information about M-shell ionization and subsequent relaxation channels is quite important in understanding double and triple ionization of krypton.

Cross sections for various channels leading to 1—4-times-ionized krypton by 10—5000-keV proton impact are presented in Fig. 7 with their sources tabulated in Table VIII. The data, although rather limited, are useful in providing some essential details about ionization of krypton. As can be seen in Fig. 7(a), multiple ionization accounts

TABLE VII. Table showing how single, double, and triple ($q=1-3$) ionization of krypton are related to initial vacancy production cross sections and to measurable final target ionization state cross sections. The relationship between these cross sections is to be read as a matrix as illustrated.

q	i	j	Initial vacancy	Subsequent processes	σ_q^T	σ_q^{11}	σ_q^{10}	σ_q^{1-1}
+1	1	1	N		1	1		
	1	0			1		1	
+2	1	1			1	1		
	1	0	N^2		1		1	
	1	−1			1			1
	1	1	$3d$	$3dNN$ Auger	a	a		
	1	0			a		a	
	1	1	$3p$	$3pNN$ Auger	b	b		
	1	0			b		b	
+3	1	1			1	1		
	1	0	N^3		1		1	
	1	−1			1			1
	1	1			c	c		
	1	0	$3dN$	$3dNN$ Auger	c		c	
	1	−1			c			c
	1	1			d	d		
	1	0	$3pN$	$3pNN$ Auger	d		d	
	1	−1			d			d
	1	1	$3d$	$3dNNN$ Auger	e	e		
	1	0			e		e	
	1	1	$3p$	$3p3dN$ Coster-Kronig plus $3dNN$ Auger,	$fc+g$	$fc+g$		
	1	0		or $3pNNN$ Auger	$fc+g$		$fc+g$	
	1	1	$3s$	$3s3pN$ Coster-Kronig plus $3pNN$ Auger, or $3s3dN$ Coster-Kronig plus $3dNN$ Auger,	$hd+ic+j$	$hd+ic+j$		
	1	0		or $3sNNN$ Auger	$hd+ic+j$		$hd+ic+j$	

e.g., $\sigma_3^{11}=\sigma_{N^3}^{11}+c\sigma_{3dN}^{11}+d\sigma_{3pN}^{11}+e\sigma_{3d}^{11}+(fc+g)\sigma_{3p}^{11}+(hd+ic+j)\sigma_{3s}^{11}$

a is the fraction of $3d$ vacancies undergoing $3dNN$ Auger delay
b is the fraction of $3p$ vacancies undergoing $3pNN$ (likely to be small)
c is the fraction of $3dN$ vacancies undergoing $3dNN$
d is the fraction of $3pN$ vacancies undergoing $3pNN$ (likely to be small)
e is the fraction of $3d$ vacancies undergoing $3dNNN$
f is the fraction of $3p$ vacancies undergoing $3p3dN$ Coster-Kronig
g is the fraction of $3p$ vacancies undergoing $3pNNN$ Auger
h is the fraction of $3s$ vacancies undergoing $3s3pN$ Coster-Kronig
i is the fraction of $3s$ vacancies undergoing $3s3dN$
j is the fraction of $3s$ vacancies undergoing $3sNNN$ Auger

for approximately half of the total ionization cross section (σ_+) throughout the entire energy range investigated. Also, it can be seen that single electron capture by the proton leads to multiple ionization of krypton essentially all of the time for proton energies above the M-shell binding energies. This is due to inner-shell capture, i.e., $\sigma^{10}=\sigma_M^{10}$ at high energies.[33]

Single ionization [Fig. 7(a)] occurs via direct N-shell ionization above approximately 100 keV and via N-shell capture for lower energies [see Table VII and Fig. 7(a)]. Cross sections for N-shell capture (σ_N^{10}), which by Table VII are seen to be equal to σ_1^{10}, fall all almost exponentially (E^{-5}) at the higher energies although a change in slope (to E^{-3}) is noted for impact velocities matching the M-shell bound electron velocity.[11–13,16] Following the argument outlined for argon, this could be attributed to a con-

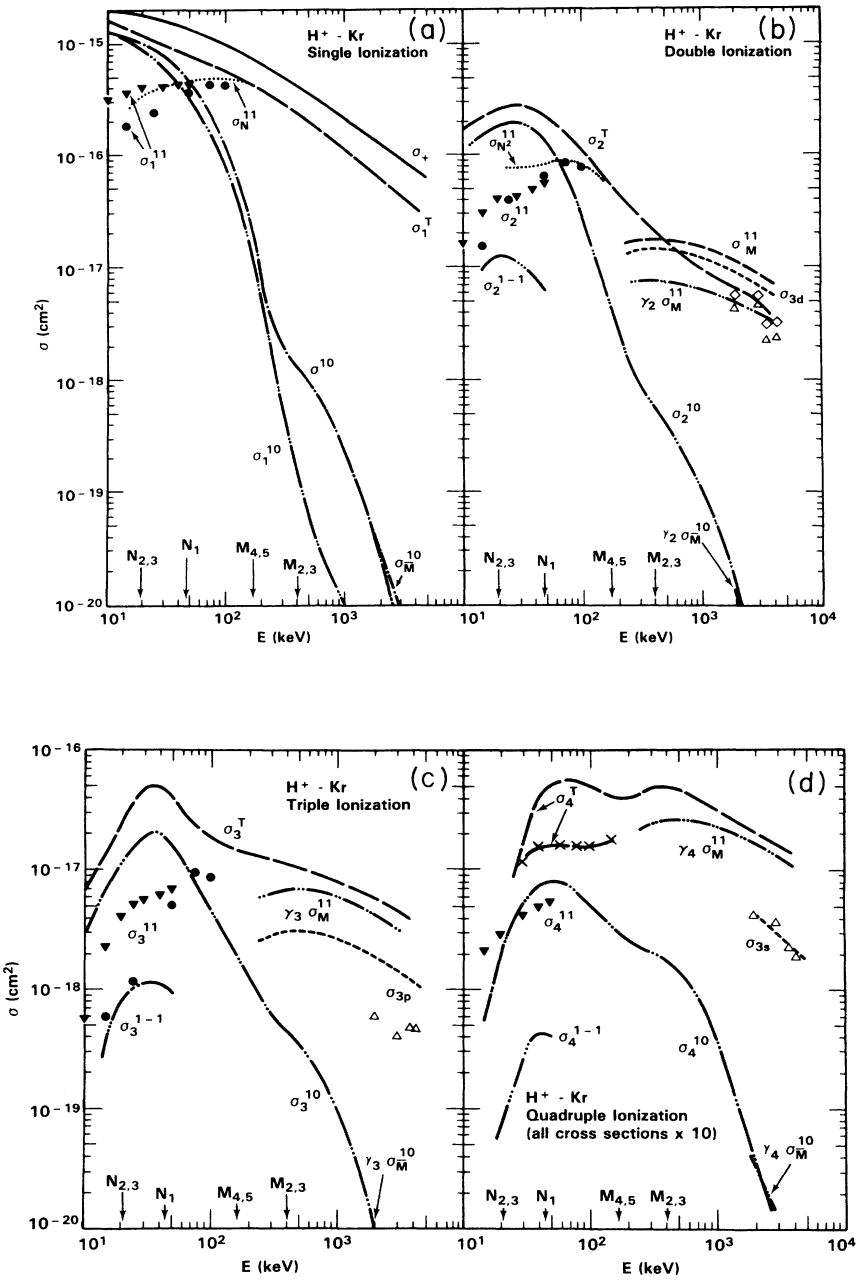

FIG. 7. Cross sections for proton impact ionization of krypton. (a) Total and single ionization. σ_+: ——, Ref. 3. σ^{10}: —·—, Refs. 5, 16, and 33. σ_1^T: ——, Ref. 6. σ_1^{10}: —··—, Refs. 11–13 and 16. $\sigma_{\bar{M}}^{10}$: —·—, Ref. 33. σ_1^{11}: ▼, Ref. 13; ●, Ref. 16. σ_N^{11}: · · · ·, from $\sigma_1^T-\sigma_1^{10}$. (b) Double ionization. σ_2^T: ——, Ref. 6. σ_2^{10}: —··—, Refs. 11–13 and 16. σ_2^{1-1}: — ··· —, Ref. 13. σ_M^{11}: — — — (theory) and ◇ (expt), Ref. 32. σ_{3d}^{11}: — — — (theory) and △ (expt), Ref. 32. $\gamma_2\sigma_M^{11}$: —··—, σ_M^{11} (theory) combined with Ref. 11. $\gamma_2\sigma_{\bar{M}}^{10}$: —··—, $\sigma_{\bar{M}}^{10}$ combined with Ref. 11. σ_2^{11}: ▼, Ref. 13; ●, Ref. 16. $\sigma_{N^2}^{11}$: · · · ·, from $\sigma_2^T-\sigma_2^{10}-\sigma_2^{1-1}-\gamma_2\sigma_M^{11}$. (c) Triple ionization. σ_3^T: ——, Ref. 6. σ_3^{10}: —··—, Refs. 11–13 and 16. σ_3^{11}: — ··· —, Ref. 13. $\gamma_3\sigma_M^{11}$: —··—, σ_M^{11} combined with Ref. 11. σ_{3p}^{11}: — — — (theory) and △ (expt), Ref. 32. $\gamma_3\sigma_{\bar{M}}^{10}$: —··—, $\sigma_{\bar{M}}^{10}$ combined with Ref. 11. σ_3^{11}: ▼, Ref. 13; ●, Ref. 16. (d) Quadruple ionization (note that the cross sections have been multiplied by 10). σ_4^T: ——, Ref. 6; —×—, Ref. 7. σ_4^{10}: —··—, Refs. 11–13 and 16. σ_4^{1-1}: — ··· —, Ref. 13. σ_{3s}^{11}: — — — (theory) and △ (expt), Ref. 32. $\gamma_4\sigma_M^{11}$: —··—, σ_M^{11} (theory) combined with Ref. 11. $\gamma_4\sigma_{\bar{M}}^{10}$: —··—, $\sigma_{\bar{M}}^{10}$ combined with Ref. 11. σ_4^{11}: ▼, Ref. 13. Cross-section nomenclature is defined in the text. Note that the theoretical σ_{3l} are for direct $3l$ vacancy production whereas the experimental values are integrated intensities of Auger transitions originating from $3l$ vacancies. See text for further explanation. Proton velocities matching those of the bound target electrons are indicated by the arrows.

TABLE VIII. Sources of the data used in Fig. 7 to describe proton impact ionization of krypton.

Cross section	Source	Comment	
σ_+	Rudd *et al.*[a]	*A* (absolute)	10–4000 keV
σ^{10}	Nakai *et al.*[b]	*C* (compilation)	0.1–4370
	DuBois[c]	*A*	15–100
	Andriamonje *et al.*[d]	*A*	2000–3000
σ_q^T	DuBois, Toburen, and Rudd[e]	*A*	10–4000
	Solov'ev *et al.*[f]	*A*	10–180
σ_q^{10}	Horsdal-Pedersen and Larsen[g]	*N* (normalized)	50–2000
	Schuch[h]	*N*	30–120
	Afrosimov *et al.*[i]	*A*	5–50
	DuBois[c]	*A*	15–100
σ_q^{11}	Afrosimov *et al.*[i]	*A*	5–50
	DuBois[c]	*A*	15–100
σ_q^{1-1}	Afrosimov *et al.*[i]	*A*	15–50
σ_M^{11}	Toburen, DuBois, and Manson[j]	theory	100–5000
		A expt (Auger)	2000–4200
σ_M^{10}	Andriamonje *et al.*[d]	theory	2000–3000
$\gamma_q\sigma_M^{11}$	Horsdal-Pedersen and Larsen[g]	*N* (branching ratios from capture)	250–2000
	Krause and Carlson[k] and Carlson, Hunt, and Krause[l]	*N* (charge state ratios)	0.1–1.4[m]
$\gamma_q\sigma_M^{10}$	Horsdal-Pedersen and Larsen[g]	*N* (branching ratios from capture)	250–2000
σ_{3l}^{11}	Toburen, DuBois, and Manson[j]	theory	100–5000
		A expt (Auger)	2000–4200

[a]Reference 3.
[b]Reference 5.
[c]Reference 16.
[d]Reference 33.
[e]Reference 6.
[f]Reference 7.
[g]Reference 11.
[h]Reference 12.
[i]Reference 13.
[j]Reference 32.
[k]Reference 25.
[l]Reference 34.
[m]For x-ray impact.

tribution to σ_1^{10} arising from *M*-shell capture followed by x-ray relaxation. However, this requires a fluorescence yield that is much too large.

Direct single-ionization cross sections ($\sigma_1^{11}=\sigma_N^{11}$ as seen from Table VII) have been measured for impact energies below 100 keV.[13,16] These cross sections agree with each other and with those obtained by subtracting σ_1^{10} from σ_1^T above 50 keV. At lower energies there is no consistency between the different σ_1^{11} cross-section measurements or with the values obtained by subtraction (dotted curve). At high energies, σ_1^{11} behaves approximately as $\ln E/E$.

Figure 7(b) presents cross sections for double ionization of krypton. As illustrated in Table VII, double ionization of krypton will occur via double *N*-shell ionization or via $3d$ ionization followed by a $3dNN$ Auger transition. $3p$ ionization does not, in general, lead to double ionization since only $\sim 1\%$ of the $3p$ vacancies relax via $3pNN$ Auger decay; Coster-Kronig transitions leading to higher stages of ionization dominate the $3p$ vacancy relaxation channels.[35] At lower impact energies, where double outer-shell ionization is most important, the charge transfer plus ionization channel (σ_2^{10}) is the most important with direct double ionization (σ_2^{11}) dominating between 100 and 500 keV. Double capture is again of little importance. The experimental measurements of direct double ionization are in good agreement with each other but tend to be smaller than the values obtained by subtraction at low impact energies. This is probably because the subtraction requires determining the small difference between two large cross sections. Thus the experimental values are expected to be more accurate below 100 keV.

Above a few hundred keV, σ_2^{10} is small [see Fig. 7(b)]. In this region $3d$ ionization followed by $3dNN$ Auger relaxation becomes extremely important as indicated by the change in slope of both σ_2^T and σ_2^{10} when the proton velocity is approximately the same as the krypton bound *M*-shell electron velocities. Since, as discussed above, $3p$ ionization does not contribute appreciably to σ_2^{11}, according to Table VII, in the higher energy region $\sigma_2^T=\sigma_2^{11}=\sigma_{N^2}^{11}+a\sigma_{3d}^{11}$. Furthermore, at the highest energies, $\sigma_{N^2}^{11}$ should not be very important since it rapidly decreases with increasing energy. Thus σ_2^T takes on the energy dependence of the $3d$ inner-shell cross section and at the highest energies shown in Fig. 7(b), to an excellent approximation, $\sigma_2^T=a\sigma_{3d}^{11}$. Using the theoretical $3d$ cross sections[32] along with the experimental σ_2^T cross sections shown in Fig. 7(b), we deduce a value of $a=0.64$, where a is the fraction of $3d$ vacancies that decay via a $3dNN$ Auger process. This is entirely consistent with a direct measurement of a.[25]

This points out that $\sim\frac{1}{3}$ of the $3d$ vacancies decay by multiple Auger processes which lead to triple or higher degrees of ionization and accounts for the discrepancy be-

tween the integrated Auger transitions associated with initial $3d$ vacancies [$\triangle$ in Fig. 7(b)] and the calculated $3d$ cross section [$- - -$ in Fig. 7(b)]. It thus demonstrates the difficulty of obtaining subshell cross sections from Auger spectra unless the spectroscopy has a large signal-to-noise ratio and is of sufficiently high resolution to identify electrons originating from multiple Auger decays.

In principle, $\sigma_{N^2}^{11}$ could now be determined for all impact energies from $\sigma_{N^2}^{11}=\sigma_2^T-\sigma_2^{10}-a\sigma_{3d}^{11}$. At lower impact energies where the $3d$ cross section is relatively small, the $\sigma_{N^2}^{11}$ obtained in this manner [dotted curve in Fig. 7(b)] is seen to be in fair agreement with the measured σ_2^{11} cross sections except in the region where the σ_2^T and σ_2^{10} cross sections are of comparable magnitude. Above 200 keV, the data are not of sufficiently accuracy to take the difference meaningfully.

A cross check on the accuracy and of our interpretation of the data can be made using the following procedure. Again we assume that when an inner shell (M shell in this case) vacancy is created in krypton, the resulting charge-state fractions will be the same whether the initial vacancy was created via a direct ionization or via a charge-transfer process. Thus the charge-transfer and the direct-ionization pathways should both produce the same M-shell plus associated N-shell vacancy ratios.

Charge-state fractions have been measured for single charge capturing collisions.[11] At higher impact energies, where M-shell capture has been shown to dominate,[33] we have deduced branching ratios (γ_q) from the data. These branching ratios, when multiplied by σ_M^{11} should be in agreement with σ_q^{11} ($q>1$) at high energies. Unfortunately, we know σ_M^{11} rather than $\sigma_{\bar{M}}^{11}$; therefore $\gamma_q\sigma_M^{11}$ should be a lower limit to σ_q^T. This is seen to be the case in Fig. 7(b) where the discrepancy is $\sim 20\%$. Thus, we would conclude that approximately 20% of the time, an initial M-shell vacancy is accompanied by N-shell vacancies. In the case of charge transfer we should find good agreement between σ_q^{10} ($q>1$) and $\gamma_q\sigma_{\bar{M}}^{10}$ which is indeed the case as seen in Figs. 7(b), 7(c), and 7(d).

Cross sections for the charge-transfer, direct ionization, and inner-shell contributions leading to triple ionization of krypton are shown in Fig. 7(c). Again, as was seen in the case of double ionization, the single charge-transfer channel dominates below 70 keV, direct triple ionization is the most important only for a brief range of energies around 150 keV and the inner-shell channel is the most important for higher impact energies. The double capture channel again plays an insignificant role.

The data, it is seen from Fig. 7(c), are sparser than for singly and doubly ionized krypton. Furthermore, there are serious inconsistencies at low energies where the sum $\sigma_3^{11}+\sigma_3^{10}+\sigma_3^{1-1}$ is less than the half of the independently measured σ_3^T cross sections. At this point, it is difficult to determine where the difficulty lies, but further measurements are clearly indicated.

In the high energy (MeV) region, the falloff of the charge-transfer channels shows that $\sigma_3^T=\sigma_3^{11}$ to very high accuracy. Also, it is expected that $\sigma_{N^3}^{11}$ becomes negligible at the very highest energies. Since the decay modes of $3s$ and $3pN$ initial vacancies rarely lead to triply ionized krypton, from Table VII we expect that at high energies $\sigma_3^T=\sigma_3^{11}=c\sigma_{3dN}^{11}+e\sigma_{3d}^{11}+(fc+g)\sigma_{3p}^{11}$ with the coefficients being defined in Table VII. In this equation, the theoretical σ_{3p}^{11} and σ_{3d}^{11} cross sections[32] are used since possible multiple Auger transitions as well as experimental difficulties preclude accurately measuring the $3l$ cross sections. The coefficient g is likely to be quite small, c and e can be estimated from the value we obtained for a, appropriately weighed to account for the available number of outer-shell electrons. This yield $c=0.76$ and $e=0.36$. Last of all, theory tells us that f is approximately 0.5. Thus at 4 MeV we obtain a value of $\sigma_{3dN}^{11}=1.6\times 10^{-18}$ cm^2. This is about $\frac{1}{4}$ of σ_{3d}^{11} which seems to be reasonable. Thus we conclude that in this energy region σ_3^T is dominated ($\sim 60\%$ of the total) by $3d$ ionization followed by a $3dNNN$ multiple Auger decay. The $3dN$ and $3p$ initial ionizations account for the remaining 40% of the cross section (~ 30 and 10%, respectively).

A lower bound for σ_3^T at high energies can be obtained from $\gamma_3\sigma_M^{11}$. This gives a result that is $\sim 20\%$ below σ_3^T which is entirely consistent with the results for doubly ionized krypton. These results strongly suggest that an M-shell vacancy is accompanied approximately 20% of the time by N-shell ionization. In the case of charge transfer, $\gamma_3\sigma_{\bar{M}}^{10}$ is in reasonable agreement with σ_3^{10}, as seen in Fig. 7(c).

Data for four times ionized krypton are given in Fig. 7(d). Here, again, we find serious inconsistencies, along with outright discrepancies between two measurements of σ_4^T at the lower energies. For a complete understanding of this energy region, further measurements are crucial. However, using the limited information available, we note that σ_4^T is effectively equal to σ_4^{11} at higher energies since σ_4^{10} is relatively small. Further, $\sigma_{N^4}^{11}$ is unimportant since σ_4^T exhibits a hump for proton velocities near those of the bound M-shell electrons. Thus above several hundred keV, the possible major contributors to σ_4^T are due to the various inner-shell decay modes; (a) σ_{3dN}^{11} followed by a $3dNNN$ double Auger decay, (b) σ_{3p}^{11} followed by a $3p3d3d$ super Coster-Kronig transition and two $3dNN$ single Auger decays, and last of all (c) σ_{3s}^{11} followed successively by a $3s3pN$ Coster-Kronig, a $3p3dN$ Coster-Kronig, and a $3dNN$ Auger decay. Using the information that we obtained from the lower stages of ionization along with theoretical Auger branching ratios, it is possible, in principle, to determine $\sigma_{3dN^2}^{11}$. However, the quality of the data available at the present time precludes obtaining meaningful results.

The value of $\gamma_4\sigma_M^{11}$ is $\sim 20\%$ below σ_4^T and $\gamma_4\sigma_{\bar{M}}^{10}\approx\sigma_4^{10}$, just as was observed for double and triple ionization. This gives further corroboration that $\sigma_M^{11}=0.8\sigma_{\bar{M}}^{11}$ and lends confidence to the measured σ_4^T cross sections at high energies.

Using the limited direct multiple-ionization information available, interaction distances for krypton are determined using Eq. (8). Except for single ionization where the subtracted curve was used, the lower energy σ_q^{11} cross sections were taken to be the experimental values of Ref. 13 with the subtracted values and the data from Ref. 16 being used for higher energies. Figure 8 shows the results

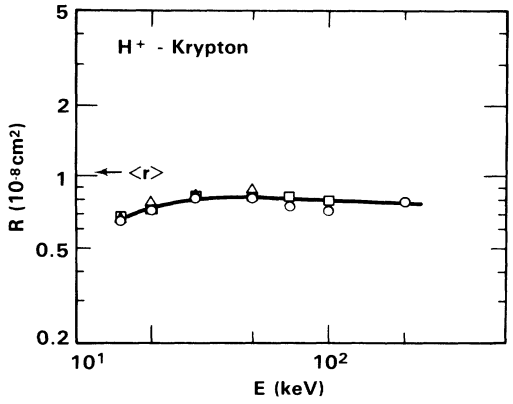

FIG. 8. Ratios of direct multiple to single outer-shell ionization cross sections for H^+-Kr collisions used for determining multiple-ionization mechanisms. Multistep mechanism: ○, □, △, for double, triple, and quadruple ionization, respectively. R is defined in Eq. (8). $\langle r \rangle$ is the Hartree-Fock value for the krypton M shell. The curve serves only to guide the eye.

obtained between 15 and 200 keV. A near constant value of 8 nm is obtained with all charge states giving similar results. This is interpreted to mean that the multistep term is dominating the perturbation expansion. Insufficient data exists to see where the single-step term becomes important. One important aspect of the same R being obtained for double, triple, and quadruple ionization is that confidence in σ_3^{11} and σ_4^{11} is obtained. These cross sections, being smaller in magnitude, are subject to larger uncertainties than are σ_2^{11}; thus R should reflect any inaccuracies in the σ_3^{11} or σ_4^{11} cross sections. That the value of R obtained in this manner is close to $\langle r \rangle$ for the N shell of krypton[15] gives further credence to the reliability of the cross sections used.

In summary, for proton impact ionization of krypton, we have shown that multiple ionization dominates the total ionization cross section. At higher energies, inner-shell ionization followed by Auger relaxation completely dominates the multiple-ionization cross section. It was found that multiple processes have appreciable effects, particularly MN and MN^2 initial ionization (similar to observations made for an argon target) and $3dNNN$ double Auger decay (confirming earlier measurements[24]).

Single-ionization cross sections are well characterized with only the low energy σ_1^{11} cross section having any significant uncertainty. Double ionization is also well characterized with only σ_2^{11} perhaps requiring further study. The situation is not so well defined for three and four times ionized krypton. Inner-shell ionization was shown to be particularly important. It is therefore essential to have better knowledge of the inner-shell cross sections and branching ratios for the decay channels than is currently available. In addition, more accurate σ_3^T and σ_4^T cross sections are necessary for a complete quantitative understanding. Nevertheless, despite these problems, we have obtained a fairly good picture of the ionization of krypton over a broad energy range.

III. FINAL REMARKS

An extensive, detailed picture of multiple ionization of helium, neon, argon, and krypton by proton impact over a broad energy range has been presented. Absolute cross sections for individual multiple-ionization mechanisms, e.g., direct outer-shell ionization, inner-shell ionization, charge transfer and charge transfer plus ionization, were obtained by combining various experimental results obtained in our laboratory or from the literature. Areas requiring additional information and areas where the existing data are not internally consistent were pointed out.

It was shown that, in general, all channels leading to ionization of helium, neon, and the lower ionization charge states of argon are known with reasonable accuracy and are internally consistent. Although it was shown that the pathways leading to multiple ionization of krypton and to the higher charge states of argon are understood, obtaining accurate cross sections for each of the individual processes will require additional inner-shell ionization cross sections and relaxation branching ratios for inner-shell vacancies.

For the cases where the available data were of sufficient accuracy to allow the determination of direct outer-shell ionization cross sections, it was shown that by using ratios of direct multiple to direct single outer-shell ionization, interaction distances could be determined. These distances were found to be approximately constant over a broad range of impact energies and independent of the multiple-ionization charge state. In these cases, it is suggested that the multistep term in the perturbation expansion should be dominant in calculating total direct outer-shell ionization cross sections for low to intermediate impact energies. Whether such an approach can also describe details of the multiple-ionization cross sections (for example, the doubly differential cross section for electron emission) cannot be determined at this time. At higher impact energies it was shown that the single-step term is becoming dominant. Thus, the cross sections presented in this paper not only provide a testing ground for present and future theoretical calculations of multiple ionization, but also provide information as to which terms in a perturbation expansion are most important.

As a final note, the importance of multiple electron processes was established. Not only multiple initial ionizations but also multiple Auger relaxations such as $3dNNN$ decay in krypton were shown to be important. These multiple processes are particularly interesting because they can only occur via correlation. Thus, they constitute particularly sensitive tests of theory.

ACKNOWLEDGMENTS

This work was supported by the Office of Health and Environmental Research, U.S. Department of Energy Contract No. DE-AC06-76RLO 1830 and National Science Foundation Grant No. PHY-8508263.

[1]J. H. McGuire, Phys. Rev. Lett. **49**, 1153 (1982); J. Phys. B **17**, L779 (1984).
[2]J. H. McGuire and L. Weaver, Phys. Rev. A **16**, 41 (1977).
[3]M. E. Rudd, R. D. DuBois, L. H. Toburen, C. A. Ratcliffe, and T. V. Goffe, Phys. Rev. A **28**, 3244 (1983).
[4]C. F. Barnett, J. A. Ray, E. Ricci, M. I. Wilker, E. W. McDaniel, E. W. Thomas, and H. B. Gilbody, Oak Ridge National Laboratory Report No. ORNL-5206, 1977 (unpublished).
[5]Y. Nakai, A. Kikuchi, T. Shirai, and M. Sataka, Japan Atomic Energy Research Institute Report No. JAERI-M 83-143, 1983 (unpublished).
[6]R. D. DuBois, L. H. Toburen, and M. E. Rudd, Phys. Rev. A **29**, 70 (1984).
[7]E. S. Solov'ev, R. N. Il'in, V. A. Oparin, and N. V. Federenko, Zh. Eksp. Tekh. Fiz. **42**, 659 (1962) [Sov. Phys.—JETP **15**, 459 (1962)].
[8]S. Wexler, J. Chem. Phys. **41**, 1714 (1964); **44**, 2221 (1966).
[9]L. J. Puckett and D. W. Martin, Phys. Rev. A **1**, 1432 (1970).
[10]H. Knudsen, L. H. Anderson, P. Hvelplund, G. Astner, H. Cederquist, H. Danared, L. Liljeby, and K.-G. Rensfelt, J. Phys. B **17**, 3545 (1984).
[11]E. Horsdal-Pedersen and L. Larson, J. Phys. B **12**, 4085 (1979).
[12]B. Schuch, Diplomarbeit, University of Giessen, 1984.
[13]V. V. Afrosimov, Yu A. Mamaev, M. N. Panov, and N. V. Federenko, Zh. Tekh. Fiz. **39**, 159 (1969) [Sov. Phys.—Tech. Phys. **14**, 109 (1969)].
[14]M. B. Shah and H. B. Gilbody, J. Phys. B **18**, 899 (1985).
[15]J. B. Mann, Los Alamos Scientific Report No. LA-3691, 1971 (unpublished).
[16]R. D. DuBois, Phys. Rev. Lett. **52**, 2348 (1984).
[17]S. T. Manson, R. D. DuBois, and L. H. Toburen, Phys. Rev. Lett. **51**, 1542 (1983).
[18]M. Rødbro, E. Horsdal-Pedersen, C. L. Cocke, and J. R. MacDonald, Phys. Rev. A **19**, 1936 (1979).
[19]N. Stolterfoht and D. Schneider, Phys. Rev. A **11**, 721 (1975).
[20]N. Stolterfoht, H. Gabler, and U. Leithäuser, Phys. Lett. **45A**, 351 (1973).
[21]A. K. Edwards and M. E. Rudd, Phys. Rev. **170**, 140 (1968).
[22]M. O. Krause, F. A. Stevie, L. J. Lewis, T. A. Carlson, and W. E. Moddeman, Phys. Lett. **31A**, 81 (1970).
[23]T. A. Carlson and M. O. Krause, Phys. Rev. **140**, 1057 (1965).
[24]M. Eckhardt and K.-H. Schartner, Z. Phys. A **312**, 321 (1983).
[25]M. O. Krause and T. A. Carlson, Phys. Rev. **149**, 52 (1966).
[26]V. V. Afrosimov, Yu A. Mamaev, M. N. Panov, and V. Uroshevich, Zh. Tekh. Fiz. **37**, 717 (1967) [Sov. Phys.—Tech. Phys. **12**, 512 (1967)].
[27]N. Stolterfoht, D. Schneider, and P. Ziem, Phys. Rev. A **10**, 81 (1974).
[28]H. Oona, Phys. Rev. Lett. **32**, 571 (1974).
[29]T. A. Carlson and M. O. Krause, Phys. Rev. **137**, 1655 (1965).
[30]R. Hippler, J. Bossler, and H. O. Lutz, J. Phys. B **17**, 2453 (1984).
[31]A. Langenberg, F. J. deHeer, and J. Van Eck, *Abstracts of the IXth International Conference on the Physics and Electronic and Atomic Collisions,* edited by J. S. Risley and R. Geballe (University of Washington Press, Seattle, 1975), p. 935.
[32]L. H. Toburen, R. D. DuBois, and S. T. Manson, IEEE Trans. Nucl. Sci. **NS-30**, 923 (1983).
[33]S. Andriamonje, J. F. Chemin, J. Roturier, B. Saboya, J. N. Scheurer, D. Z. Belkic, R. Gayet, A. Salin, H. Laurent, and J. P. Schapira, J. Phys. (Paris) **46**, 349 (1985).
[34]T. A. Carlson, W. E. Hunt, and M. O. Krause, Phys. Rev. **151**, 41 (1966).
[35]T. A. Carlson, *Photoelectron and Auger Spectroscopy* (Plenum, New York, 1975), p. 284.